JPL NO. 9950-845

DRL 126
DRD Se 8

DOE/JPL-955567-83-11
Distribution Category UC-63

TRIANNUAL REPORT

on the

DESIGN, ANALYSIS AND TEST VERIFICATION OF ADVANCED ENCAPSULATION SYSTEMS

For Period Ending

31 March 1983

Contract 955567

Prepared by:

Alexander Garcia III
James M. Kallis
D. Charles Trucker

Approved by:

Nick Mardesich
Manager, Advanced Programs

SPECTROLAB, INC.
12500 Gladstone Avenue
Sylmar, California 91342

June 1983

The JPL Flat-Plate Solar Array Project is sponsored by the U.S. Department of Energy and forms part of the Solar Photovoltaic Conversion Program to initiate a major effort toward the development of low-cost solar arrays. This work was performed for the Jet Propulsion Laboratory, California Institute of Technology by agreement between NASA and DOE.

TABLE OF CONTENTS

Section 1.0

SUMMARY

The final report on the Electrical Isolation Analysis was completed and is included as Appendix A. Several full size qualification modules were constructed using polyurethane encapsulant and a Tedlar front cover.

Section 2.0

INTRODUCTION

This program will develop the analytical methodology for advanced encapsulation designs. From these methods design sensitivities will be established for the development of photovoltaic module criteria and the definition of needed research tasks.

The program consists of four phases. In Phase I analytical models were developed to perform optical, thermal, electrical and structural analyses on candidate encapsulation systems. From these analyses several candidate encapsulation systems were selected for qualification testing during Phase II. Additionally, during Phase II test specimens of various types will be constructed and tested to determine the validity of the analysis methodology developed in Phase I.

During Phase III the following items will be covered:

1. Correction of identified deficiencies and/or discrepancies between analytical models developed during Phase I and relevant test data obtained during Phase II of the above contract.

2. Improvement and extension of prediction capability of present analytical models.

3. Generation of encapsulation engineering generalities, principles, and design aids for photovoltaic module design.

From these items the sensitivity of module performance to various material properties will be determined. This study will enable the intelligent direction of research into assessment of module life potential by analyzing those materials and their properties which through aging would most influence module performance.

In Phase IV a final optimum design based on knowledge gained in Phases I, II and III will be developed and delivered to JPL.

Section 3.0

TECHNICAL DISCUSSION

3.1 Electrical Report

NASTRAN is a comprehensive finite element computer program normally used to analyze the structural and thermal aspects of complex systems. One of the attractive features of NASTRAN is the ability to quickly and easily construct complex 3-D models. Electric fields are analogous with thermal fields and can be calculated with a thermal analyzer program such as NASTRAN. Several analyses have been done using this technique. The final report on the electrical analyses is presented as Appendix A.

3.2 Module Construction

Test panels were made using a new lot of Z-2591A polyurethane. This batch of the A part had a nonyellowing artioxidant. The panels were extremely slow in curing and showed bubble formation with time. After consulting with Development Associates, a new lot of Part A was procured with a faster cure time.

Additionally, the tanks containing the urethane components were plumbed into the house vacuum system. This storage under vacuum was successful in alleviating problems of bubbling. Several test coupons were made and showed no signs of bubble formation.

Two polyurethane modules were constructed using Tedlar as a top cover. The first module showed no signs of urethane-produced bubbling, however there were bubbles present which had come from beneath the cells.

To avoid problems with bubbles trapped beneath cells, a modified process for assembly of the polyurethane layup was developed. The procedure follows:

1. The hardboard was prepared with wood ribs epoxied to the 1/8" 4' x 4' board.

2. Strips of 20 CP 3120 polyester film (3M) were glued to the back of the substrate using 4910 pressure sensitive adhesive (3M).

3. The top of the substrate was spray painted with Krylon interior/exterior enamel 1502 (Borden). This is an alkyd-based flat white paint.

4. Holes were made in the substrate for electrical termination.

5. The substrate was placed ribs down and a layer of .003 Crameglas 230 placed upon it.

6. The surface was flooded with polyurethane.

7. The primed cell circuit was then placed on a board, one end of the circuit lightly held, and the board slowly pulled away to allow the circuit to fall on the flooded surface.

8. Additional polyurethane was then pumped on the layup until the surface was completely covered.

9. Another layer of .003" Craneglas was placed on the surface.

10. Primed (Dow Corning Z6020 5% in methanol) Tedlar 100BG 30UT was then rolled onto the layup to complete the module.

11. A weighted steel plate was placed on the module and the polyurethane allowed to cure.

This module was the most successful to date. Only a very few bubbles marred its appearance. One problem was that bubbles became trapped under the first layer of Craneglas. This will be overcome in the future by first flooding the surface with urethane and then applying the Craneglas. This technique was very successful for the second layer.

Section 4.0

CONCLUSIONS AND RECOMMENDATIONS

There are no conclusions and recommendations for this period.

Section 5.0

PLANNED ACTIVITIES

During the next period construction of the qualification modules will continue. The thermal, structural, and optical final reports will be completed.

APPENDIX

ELECTRICAL ISOLATION ANALYSIS

James M. Kallis and D. Charles Trucker
Hughes Aircraft Company
El Segundo, California

March 1983

TABLE OF CONTENTS

LIST OF ILLUSTRATIONS

LIST OF TABLES

SUMMARY

The thrust of the electrical isolation analysis performed in this phase of the encapsulation contract was to develop a method for evaluating the multidimensional effects of the module conductor geometry on the electric field. The electrical stress intensification at edges and corners of the solar cells is not predicted by the simple series capacitance model developed in the first phase of the contract. The multidimensional electric field was calculated with the finite-element-based NASTRAN Thermal Analyzer, using the analogy between thermal and electrostatic fields. To evaluate the maximum electric field accurately, the NASTRAN output had to be post-processed; a polynomial was fit to the predicted values of potential as a function of distance from the cell surface by the method of least squares, and the surface field was calculated from the best-fit polynomial. The accuracy of this method was verified by comparison with an exact solution for a geometry similar to that of typical solar cells. Two sample geometries were analyzed — a square test coupon used in electrical isolation tests performed earlier in this contract and a family of disc-shaped solar cells. These sample analyses demonstrated that this finite-element method is a useful design tool for evaluating candidate module encapsulation designs. They also showed geometric limits for which the model incurs numerical difficulties: 1) cells having very sharp edges, 2) cells much thinner than the dielectric pottant layer, and 3) cells much thicker than the dielectric pottant layer. These limits, some of which occur with advanced thin-film device modules, would require larger, specially designed computer models. It is recommended that electrical isolation analysis models suitable for advanced thin film device modules be developed.

1.0 INTRODUCTION

1.1 BACKGROUND

Electrical safety is an important factor in the design of terrestrial photovoltaic modules, in which solar cells may operate at potential differences of several thousand volts relative to ground. Electrical breakdown could be a serious hazard to people (for example, to a worker cleaning a module) and to the hardware. Modules are required to be able to withstand at least 3000 Vdc without the occurrence of breakdown (References 1 and 2).

Short-circuit paths might be, for example, the pottant and organic front cover material in a substrate module, the pottant and wood-product/load-bearing member of a wood substrate module, or the pottant between the cell and metal-foil back cover of a glass superstrate module. In addition, manufacturing defects such as cracks and bubbles will have a deleterious effect on the ability of a module to withstand high voltage stresses. Therefore electrical isolation is a key factor in the design of the module encapsulation system.

Accordingly electrical isolation has been investigated throughout this encapsulation contract. In the first part of the contract, a simple series capacitance model (shown in Figure 1) and a simple series resistance model were developed for determining the electric field strength in each material layer of the encapsulation system (Reference 3). These calculations were employed to specify the minimum layer thicknesses required to keep the electric field in each layer lower than the dielectric strength of the material in that layer (assuming that there are no flaws or manufacturing defects). In the second part of the contract, the breakdown voltage was measured for specially designed test coupons employing simulated solar cells (see Figure 2) and a variety of encapsulation schemes, and these measurements were compared with the predictions of the series capacitance model (Reference 4). The key results were as follows (see Table 1):

- For most of the encapsulation schemes tested, the breakdown voltages predicted for a particular scheme were within the range of the values measured for the test coupons of that scheme.

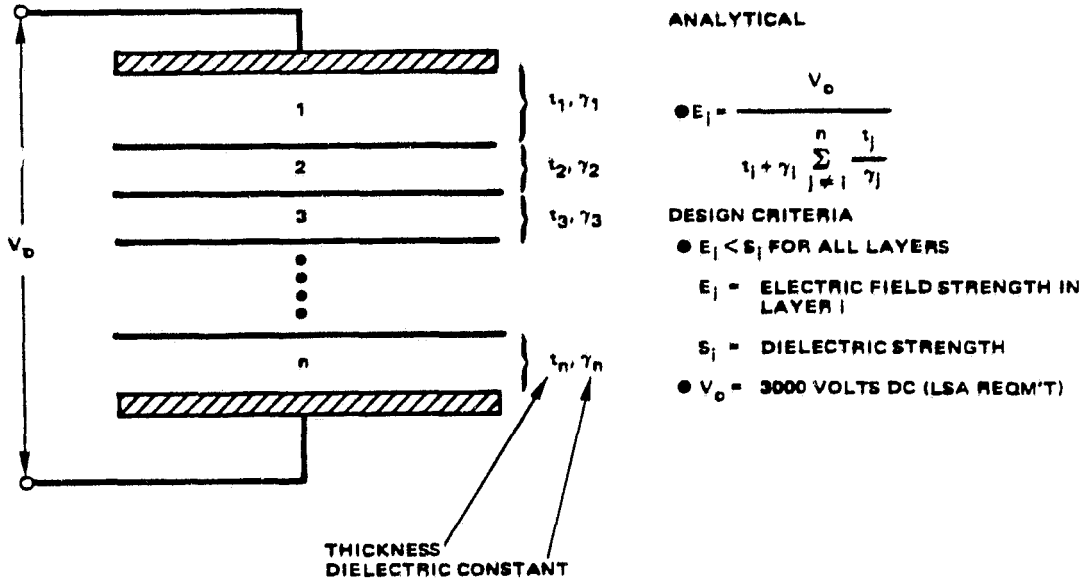

Figure 1. Series capacitance model developed in first part of contract for determination of electric isolation characteristics of photovoltaic modules.

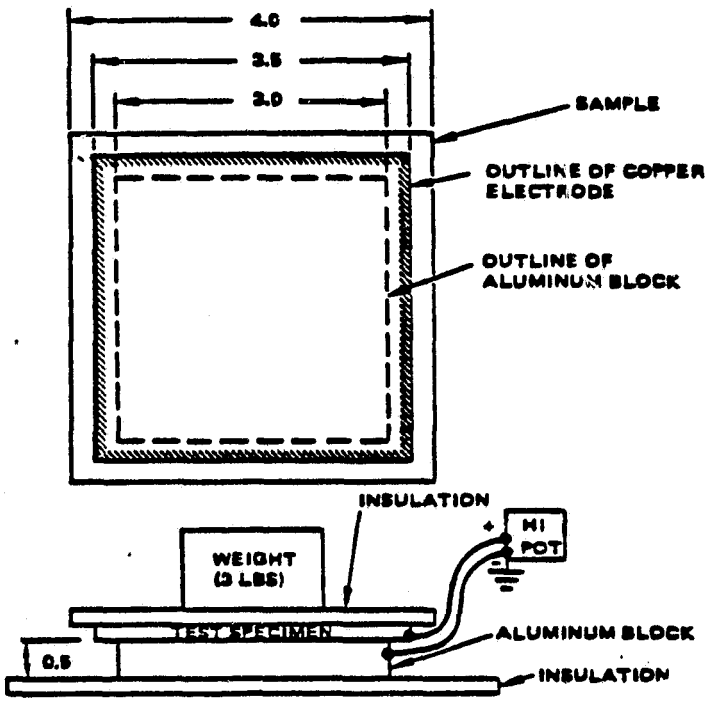

Figure 2. Test set-up for electrical isolation tests performed in second part of contract; dimensions in inches.

TABLE 1. COMPARISON OF PREDICTED AND MEASURED VALUES OF V_o AT BREAKDOWN

Coupon Type	Size	Description	V_o at Breakdown, kV			
			Measured		Predicted with Series Capacitance Model	
			Max.	Min.	Max.	Min.
A	Front	4 mil Tedlar, 18 mil EVA/CG*	19	10	14	11.8
	Back	18 mil EVA/CG, 1 mil Al Polyester*	11	1	11.2	11.2
B	Front	1 mil Tedlar, 18 mil EVA/CG	19	12	11.4	11.3
	Back	36 mil EVA/CG, 1 mil Al Polyester	13	5	22.3	22.3
C	Front	1 mil Tedlar, 18 mil EVA	21	5	11.4	11.3
	Back	18 mil EVA/CG, 125 mil wood	25	8	24.3	23.9
D1	Front	1 mil Tedlar, 36 mil EVA/CG	25	12	22.6	22.5
	Back	36 mil EVA/CG, 125 mil wood	25	21	26.8	26.0
D2	Front	1 mil Tedlar, 36 mil EVA	23	10	22.6	22.5
	Back	36 mil EVA/CG, 125 mil wood	25	22	26.8	26.0

*EVA/CG = EVA with Cranaglas
Al Polyester = Aluminized Polyester

- On the other hand, the measured breakdown-voltage ranges were much wider than those predicted by substitution of the known material-property ranges into the series capacitance model.
- The measured breakdown voltages had a weaker dependence on the pottant thickness than predicted by the series capacitance model.
- All the electrical failures occurred at the edges of the simulated solar cells in the test specimens.

These results indicated the need for a more realistic model than the series capacitance model. The series capacitance model assumes that the electric field is uniform in a layer, that is, that the lines of force are straight

and that the equipotentials are equally spaced parallel planes. Actually the equipotentials crowd together at sharp edges and corners of the cell, as shown in Figure 3. Consequently the electric field, which is the gradient of the potential, has its maximum magnitude at such locations. In the absence of flaws, the onset of breakdown can be expected to be governed by and to occur at such sharp edges and corners. This conclusion is well known (Reference 5) and is consistent with the results of the aforementioned tests performed in this contract. Therefore a realistic model must account for the multidimensional effects of the module conductor geometry on the electric field.

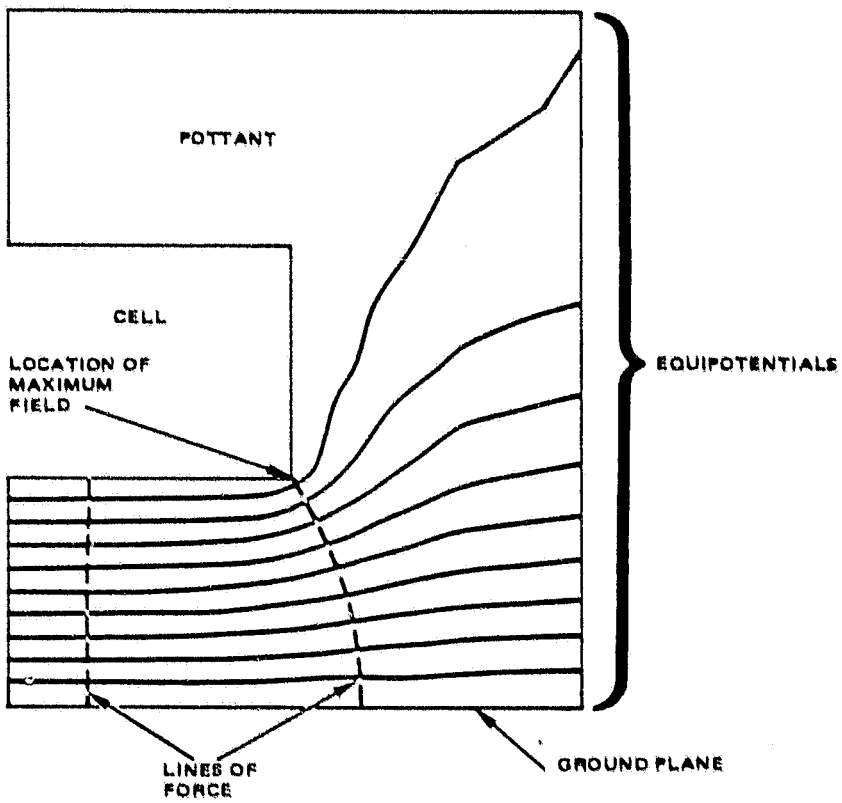

Figure 3. Electric field distribution in module.

1.2 HEAT TRANSFER ANALOGY

Fortunately three-dimensional electrostatic fields can be calculated by available heat transfer computer programs, because of the analogy between thermal and electrostatic fields (see Figure 4). Laplace's equation governs both the temperature distribution in conduction heat transfer and the potential field in electrostatics. The electric field, the quantity of interest in the electrical isolation analysis, is analogous to the temperature gradient. Because of this analogy, L. B. Duncan of Hughes suggested using the NASTRAN Thermal Analyzer computer program to calculate the electric-field enhancement resulting from candidate encapsulation schemes.

- DIFFUSION EQUATIONS

$\nabla \cdot \epsilon \nabla V + \rho = 0$ ELECTRICAL

$\nabla \cdot k \nabla T + \dot{q} = \rho c \left(\frac{\partial T}{\partial t}\right)$ THERMAL

THERMAL PARAMETER		ELECTRICAL PARAMETER	
TEMPERATURE	T	POTENTIAL	V
THERMAL CONDUCTIVITY	k	PERMITTIVITY	ϵ
TEMPERATURE GRADIENT	∇T	ELECTRIC FIELD	$\vec{E} = -\nabla V$
HEAT FLUX	$-k \nabla T$	ELECTRIC DISPLACEMENT	$\vec{D} = \epsilon \vec{E}$
INTERNAL HEAT GENERATION	$\dot{q}$	CHARGE DENSITY	$\rho = \nabla \cdot \vec{D}$

Figure 4. Thermal-electrical analogy.

1.3 PRESENT INVESTIGATION

Accordingly, an investigation of the feasibility of performing electric field analyses for photovoltaic module geometries was performed. This investigation is the subject of this report.

The specific tasks were as follows:

1) Review the literature on previous electrical analyses performed with finite-difference or finite-element computer programs using the heat transfer analogy.

2) Formulate and solve multidimensional sample problems to check the aforementioned series capacitance model and to investigate edge and corner effects.

The literature search showed that the finite-element method, employed in NASTRAN to solve the partial differential equations governing thermal and structural phenomena, has been employed to calculate electric fields since the late 1960s. Books have been written on the method (for example, Reference 6), and the MSC/NASTRAN program used for thermal and structural analyses at Hughes has been employed for electrical analyses (References 7 and 8). These findings indicated the likely success of the application of this method to the photovoltaic module electrical isolation analysis.

The remainder of this report describes this application. Section 2 describes the development, verification, and use of the method. Section 3 describes the sample geometries analyzed and the results. And Sections 4 and 5 present conclusions and recommendations.

2.0 METHOD

2.1 NASTRAN THERMAL ANALYZER

The finite-element-based NASTRAN Thermal Analyzer (Reference 9) is a general-purpose heat transfer computer program. As an integrated part in the NASTRAN (NASA structural analysis computer program) system, this thermal analysis capability is fully capable of rendering temperature solutions and heat flows in solids subject to various boundary conditions, which range from prescribed temperatures at grid points and specified thermal loads to convective and radiative modes of heat transfer at boundary surfaces in both steady-state and transient cases. This heat transfer computer program has been developed by an application of existing functional modules in NASTRAN, which were designed originally for the purpose of structural analysis, and the addition of new modules including new elements and new solution algorithms.

2.2 CALCULATION OF MAXIMUM FIELD

The quantity of interest for the photovoltaic module electrical isolation analysis is the maximum electric field in the module. For the geometry shown in Figure 3, the maximum field occurs at the cell edge or corner, and the field vector there is perpendicular to the cell surface. For a finite edge or corner radius of curvature, the precise location of the maximum field is not known a priori. The problems attacked here were to locate and evaluate the maximum field from the NASTRAN output, namely, the average potential in each of the analysis elements.

This endeavor was not straightforward. NASTRAN calculates the field simply by

$$E_{NASTRAN} = \Delta V/d \ ,$$

where ΔV = potential difference between adjacent analysis elements and
d = spacing between these elements.

This formula significantly underestimates the surface field because, as seen in Figure 3, the potential is a nonlinear function of the distance D from the cell surface. In other words, the function V(D) has a non-zero second derivative. Trial computer runs indicated that the field computed by NASTRAN underestimated the surface field and that the use of a finer computational mesh or modifications in the shape of the mesh did not solve the problem.

The successful solution was to:

1) Calculate the potential distribution with a moderate size (around 500 elements) NASTRAN model,
2) Perform a least-squares curve fit to the NASTRAN output values of the function V(D), and then
3) Calculate the surface field from the best-fit formula.

The development of this procedure is described in Appendix A.

2.3 VERIFICATION OF METHOD

A geometry, similar to those of interest for photovoltaic applications, for which there is an exact solution of Laplace's equation was discovered.

This geometry consists of an infinitesimally thin planar electrode (V = 1) located halfway between two ground planes. The high-voltage electrode extends to infinity toward the right, and the ground planes extend to infinity toward the left and the right. The equipotential surfaces asymptotically approach parallel planes and can be described as blunted knife-edged slabs. The details of this exact solution are described in Appendix B.

The equipotentials resemble the shapes of solar cells and thus can serve as a model of solar cells having axial symmetry (discs) or cells having planar geometry (strips). Any equipotential can be thought of as the surface of a solar cell.

To verify the aforementioned method for calculating the maximum electric field, a NASTRAN model of the blunted knife-edged slab was developed for the region between the V = 0.8 equipotential surface and the ground plane. This surface and two other equipotentials are plotted in Figure 5. The geometry corresponds to a ratio of cell thickness to pottant thickness having the value $t_c/t_p = 0.5$. The NASTRAN model had 264 elements and 308 grid points. The maximum field occurs at the surface halfway between the ground planes.

The maximum fields predicted by the exact solution and by the best-fit polynomial to the NASTRAN output agreed to within 3 decimal places, which is remarkably close agreement. The potential distributions predicted by the exact solution and by NASTRAN also agreed very closely, as shown in Figure 6.

This excellent agreement with the exact solution verifies the accuracy of the method described in the previous section for calculating the maximum field. It also indicates that a moderate-size model consisting of a few hundred analysis elements provides sufficient accuracy for typical geometries of interest.

2.4 USE OF METHOD

This method can be used in providing for the electrical isolation of photovoltaic modules as follows. To avoid breakdown, the module should be designed so that

$$E_m < S, \qquad (1)$$

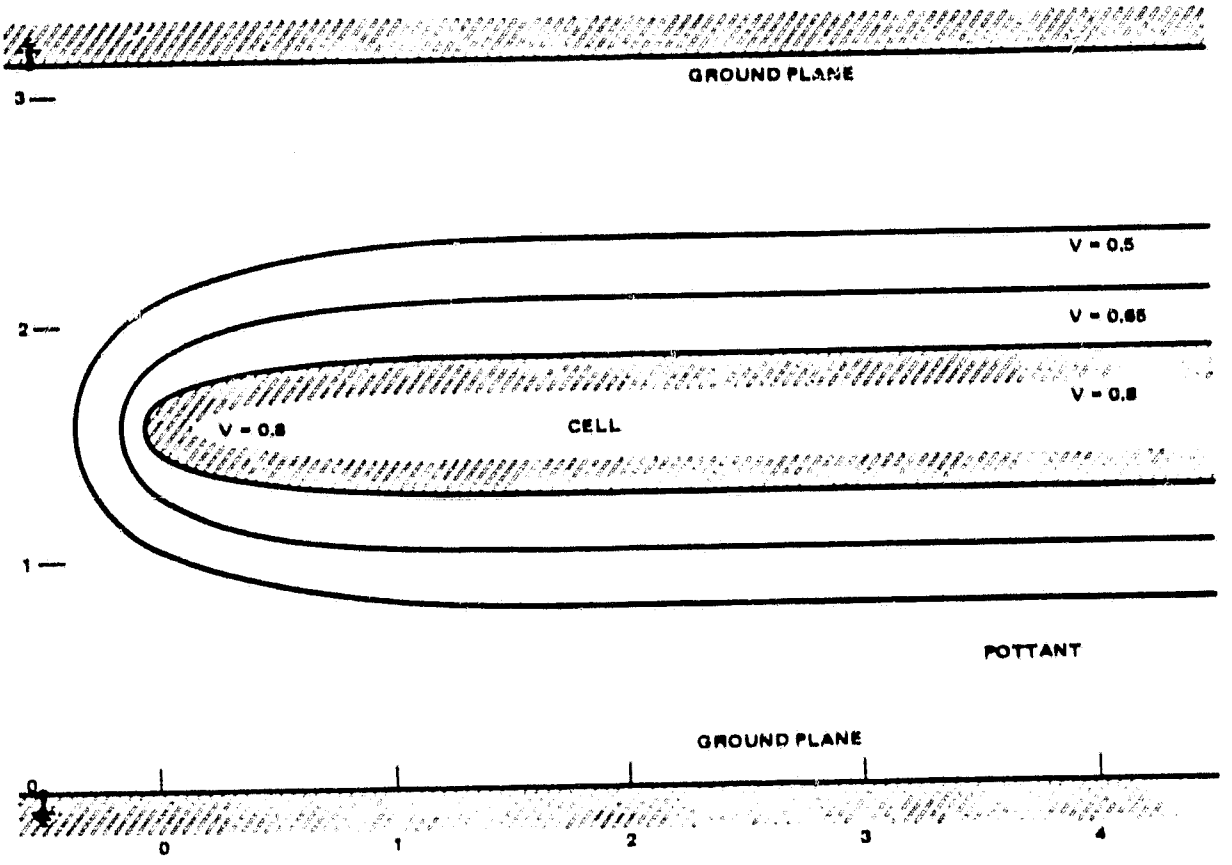

Figure 5. Blunted knife-edged slab, exact solution ($t_c/t_p = 0.5$).

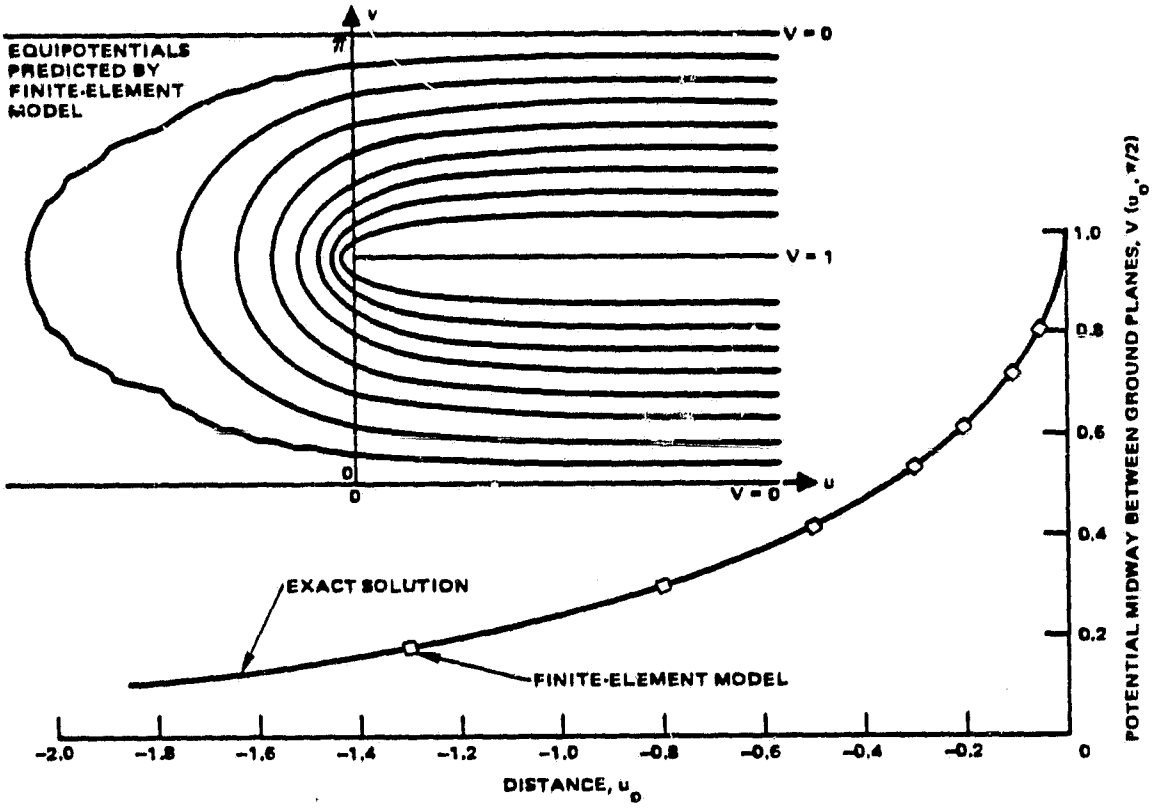

Figure 6. Potential distribution for blunted knife-edged slab.

where

E_m = maximum electric field in module and

S = dielectric strength of pottant.

The maximum field is a function of the following parameters:

- The voltage difference V_o between the solar cell and the ground plane (the modules are required to withstand a voltage difference of at least 3000 Vdc without breaking down),
- The thickness t_p of the pottant, and
- The geometry of the module (specifically, the effects of sharp edges or corners on conductors).

In the previous series capacitance model, the electric field in each layer was assumed to be given by the value for infinite parallel plates:

$$E_{pp} = V_o/t_p. \tag{2}$$

(This is a good approximation to the field except near edges and corners of conducting surfaces.) This enabled the minimum allowable pottant thickness to be calculated by

$$E_{pp} < S, \text{ (series capacitance model)} \tag{3}$$

which yields

$$t_p > V_o/S. \text{ (series capacitance model)} \tag{4}$$

With the present method, we define y as the ratio of the field for infinite parallel plates to the maximum field:

$$y = \frac{E_{pp}}{E_m} = \frac{V_o/t_p}{E_m}. \tag{5}$$

The quantity y, which is a function only of the module geometry, is an electrical stress intensification factor. It indicates the amount by which the module's voltage-withstanding capability is reduced because of sharp edges or corners. For example, if y = 0.7, the maximum field in the module would exceed the pottant's dielectric strength at a voltage difference 70% as large as would be predicted by the series capacitance model. Thus the method described herein for calculating the maximum field can be employed to evaluate the electrical isolation characteristics of candidate module geometries, as well as to specify the minimum allowable pottant thickness. The design criterion, replacing (4), is

$$y\ t_p > V_o/S. \tag{6}$$

This method does not predict the voltage at which breakdown will occur across the entire pottant layer for a given module. Rather it predicts the voltage at which breakdown could begin in a microscopic region. Prediction of the development of this onset of breakdown into a conductive path across the entire pottant layer involves complicated phenomena (see Reference 5) and would be a big step beyond the present analysis. The work reported herein was limited to the method for predicting the electrical stress intensification factor y.

3.0 ANALYSIS OF SAMPLE GEOMETRIES

3.1 SQUARE ELECTRICAL ISOLATION TEST COUPON

The first sample geometry analyzed was a typical test coupon used in the electrical isolation tests performed earlier in this contract and reported in Reference 4. The back side of coupon Type A (see Table 1) was modelled. The copper test coupon and the finite-element model of the corner region are shown in Figure 7. The analysis model consisted of 520 elements and was constructed so that the radius of curvature of the corner in the plane of the coupon could be varied as a parameter. The edges of the coupons were assumed to be infinitely blunt. (The radii of curvature of the corners and edges of the actual test coupons were never measured, and no information on typical values was available.)

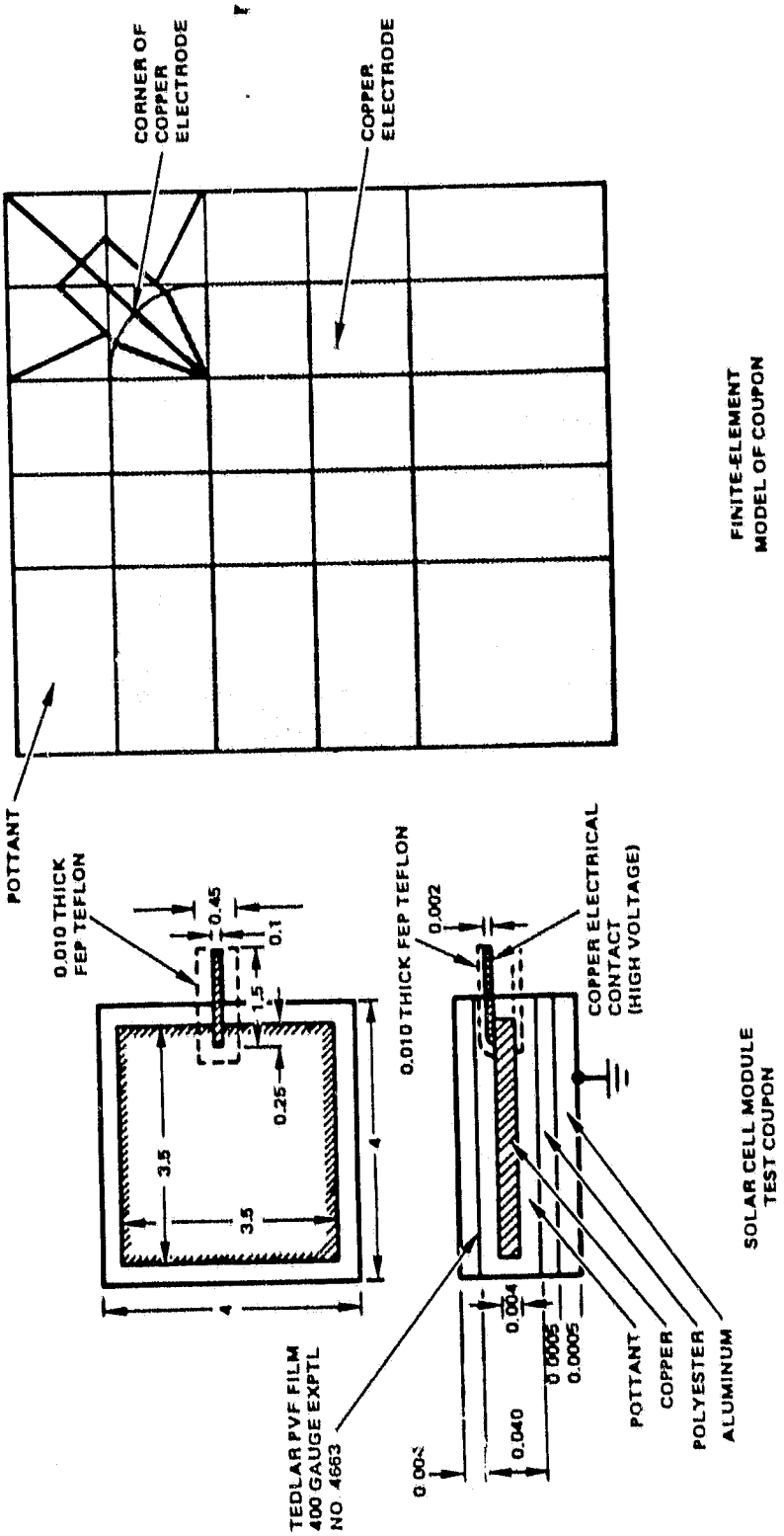

Figure 7. Electrical isolation test coupon and finite-element model of it.

The predicted electrical stress intensification factor y is plotted versus the ratio of the radius of curvature of the test coupon to the pottant thickness in Figure 8. The curve appears to behave correctly in the limits:

- $y \to 0$ as $R/t_p \to 0$,

that is, the electric field becomes infinite in the limit of a perfectly sharp corner

- $y \to 1$ as $R/t_p \to \infty$,

that is, the electric field approaches the value for parallel plates in the limit of a very blunt corner.

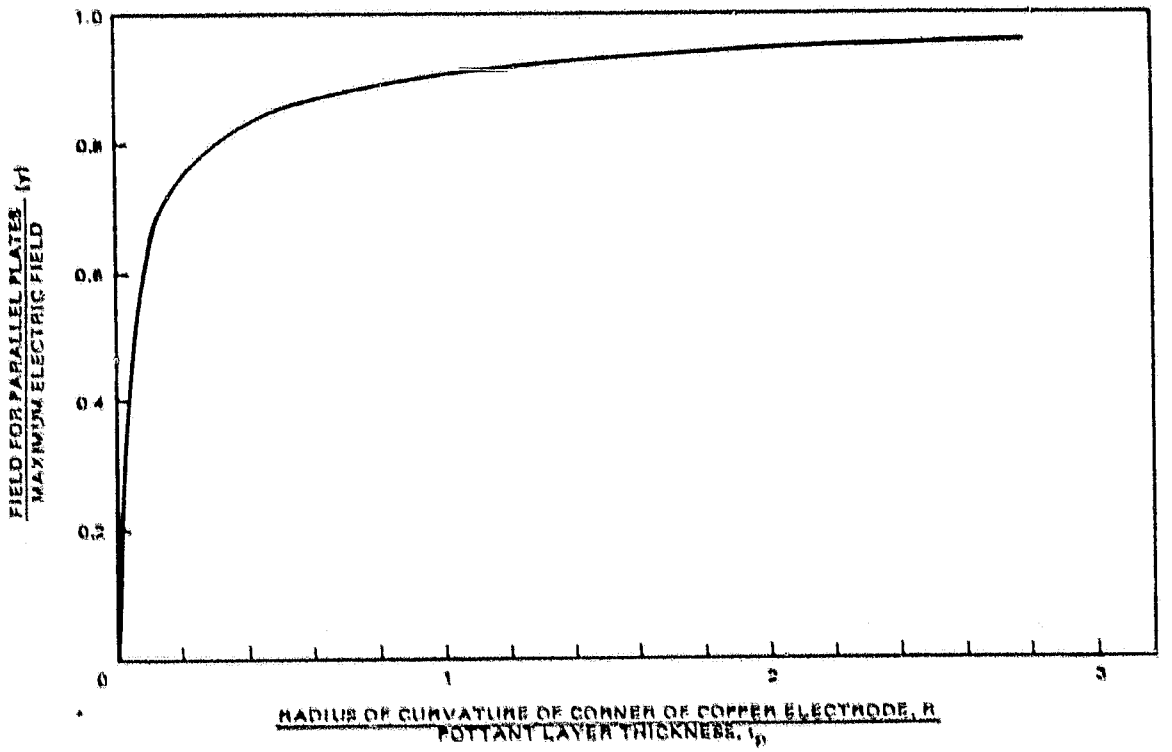

Figure 8. Square test coupon -- effect of coupon corner radius of curvature on electrical stress intensification factor.

The test data listed in Table 1 are for the voltage at which the entire layer broke down, not the voltage at which the breakdown began in a small region, and are not comparable with the predictions of the present analysis.

3.2 DISC-SHAPED SOLAR CELL

The other sample geometry analyzed was the family of disc-shaped solar cells shown in Figure 9. The radius of curvature R of the sun-side edge was assumed to be the same as that of the other edge. The electrical stress intensification factor y is a function of the parameters R/t_c and $x(=t_p/t_c)$, where t_c = cell thickness. As shown in Figure 9, R/t_c varies between the values 0 (the limit of a perfectly sharp edge) and 0.5 (the limit of a semicircular edge having no flat portion). The scale drawings below the abscissa in the figure illustrate the edge shapes for various values of R/t_c.

This family was selected for analysis because it is a good model of present and future solar cells. Of particular interest were the following limits:

- $R/t_c \to 0$.

This is a sharp-edged cell (see Figure 10) and represents the limit of the type that is produced currently by single-crystal growth and laser scribing. On physical grounds, we expected that $y \to 0$ as $R/t_c \to 0$, that is, the maximum electric field is infinite for a perfectly sharp edge.

- $t_c/t_p \to 0$ for $R/t_c = 0.5$.

This is a thin, blunt-edged cell (see Figure 10) and represents advanced thin-film devices. We held $R/t_c = 0.5$ because it seems implausible that the edge of a thin-film cell will have a flat portion.

- $x\ (=t_p/t_c) \to 0$ for $R/t_c = 0.5$.

This is the limit of a very thick, blunt cell or the limit of a very thin dielectric layer. We expected on physical grounds that $y \to 1$ as $x \to 0$, that is, the maximum electric field approaches the parallel-plate value for an infinitely blunt cell.

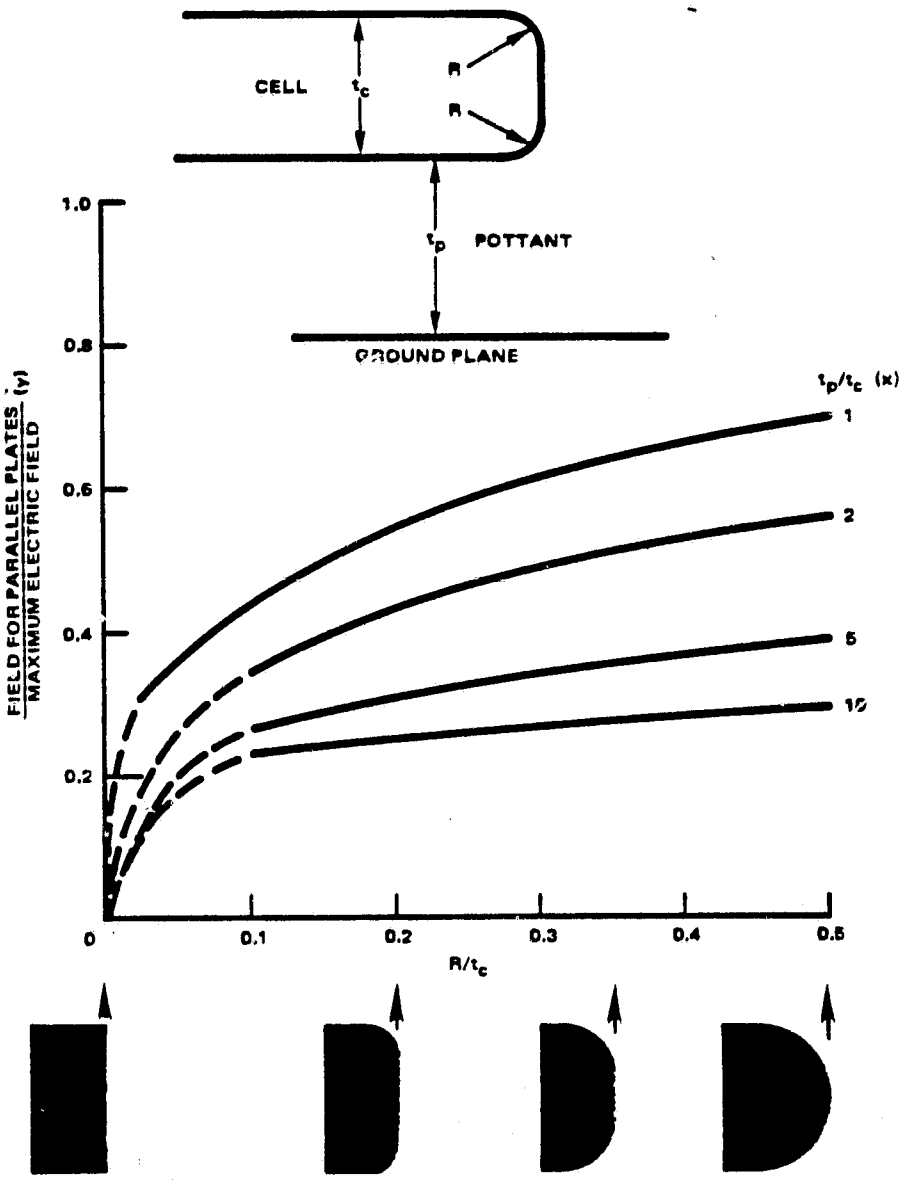

Figure 9. Disc-shaped cell – effect of cell edge radius of curvature on electrical stress intensification factor.

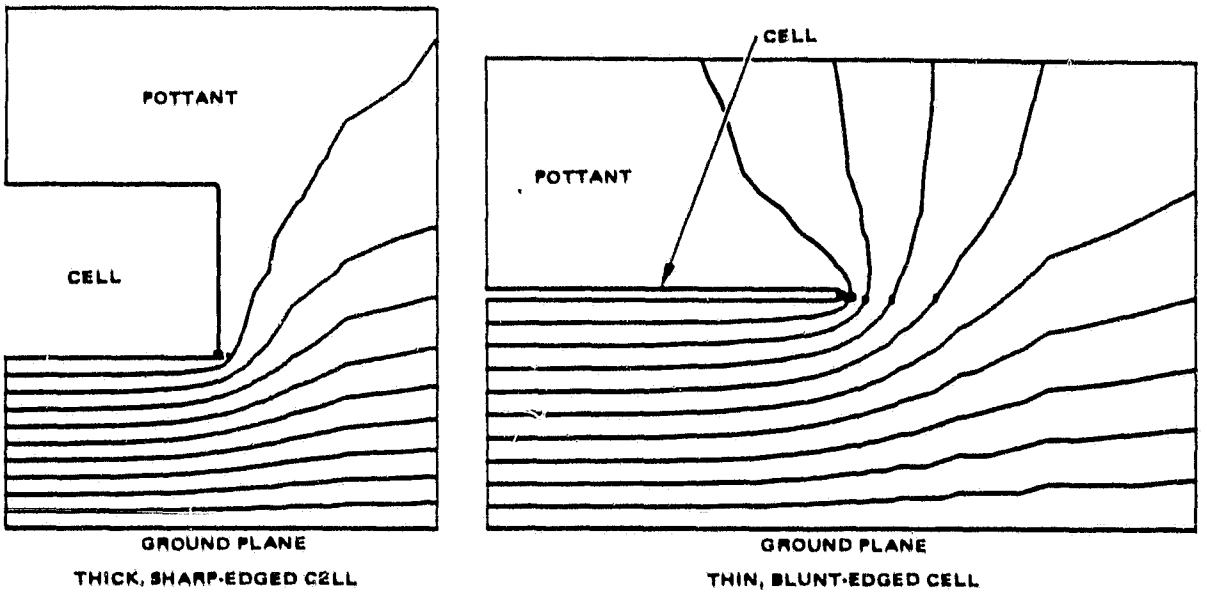

Figure 10. Typical plots of equipotentials for disc-shaped cell.

The analysis model consisted of approximately 400 elements and 460 grid points. It was constructed so that R/t_c and x could be varied as parameters.

Figure 9 shows the predicted dependence of y on R/t_c for several values of x. In accord with our aforementioned expectation, the computed curves (shown as solid curves) have been extrapolated as dashed curves to the origin. As explained in Appendix A, the model incurs numerical difficulties for small values of R/t_c (sharp edges) and large values of x (thin cells). Some of the results in these regimes appeared physically wrong and were not used. The model could be extended to these regimes in the future.

Figure 11 shows the dependence of y on t_c/t_p, for $R/t_c = 0.5$ (a semicircular edge). The scale drawings below the abscissa show the geometry for

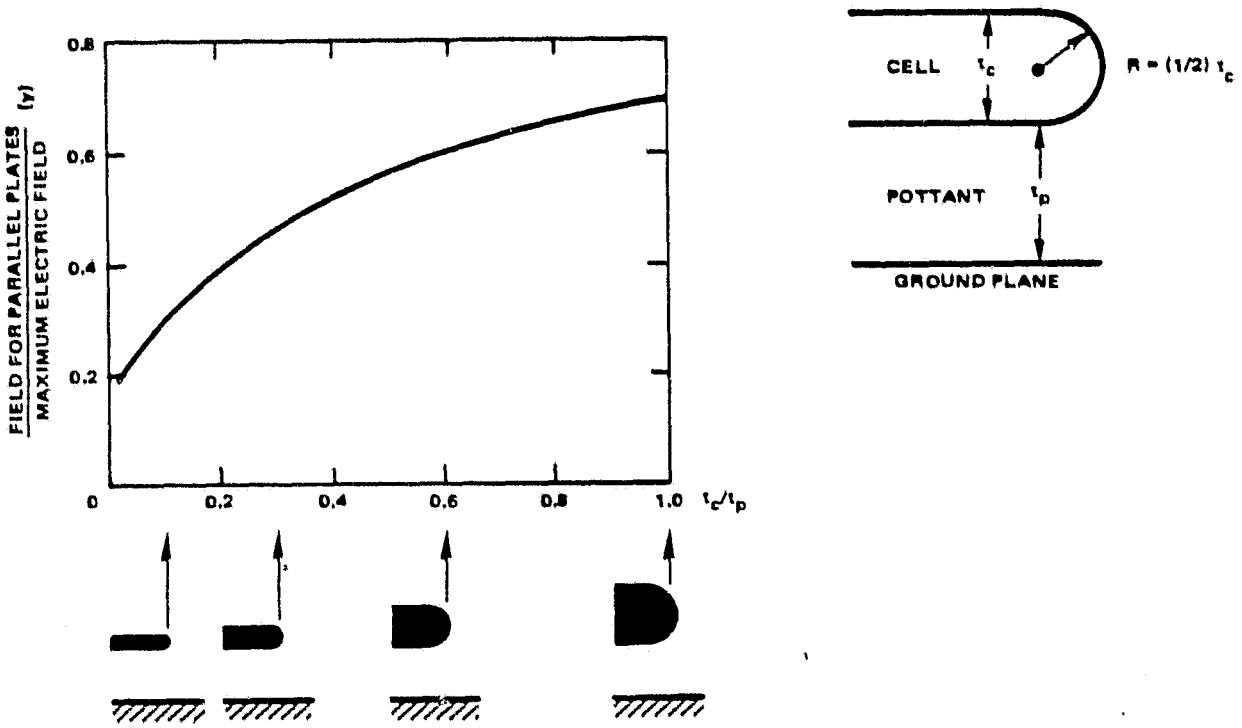

Figure 11. Disc-shaped cell — effect of cell thickness on electrical stress intensification factor.

various values of t_c/t_p. For the thinnest cell analyzed ($t_c/t_p = 0.02$ ($x = 50$)), $y = 0.19$; that is, the maximum electric field is approximately five times as high as for parallel plates having the same spacing. For such a small value of t_c/t_p, the model has numerical difficulties, and it is difficult to determine the limit of y as $t_c/t_p \to 0$. This limit, which is important for advanced thin-film solar cells, could be evaluated by further work on the model.

To determine the limit as $x \to 0$, we plotted y versus x in Figure 12. As was mentioned previously, we expected on physical grounds that $y \to 1$ as $x \to 0$. Calculated values for $x \geq 0.5$ ($t_c/t_p \leq 2$) do indeed appear to lie on a curve that is approaching the (0,1) point. We also computed the value for $x = 0.25$ ($t_c/t_p = 4$), and it falls near this curve. However, the present model begins

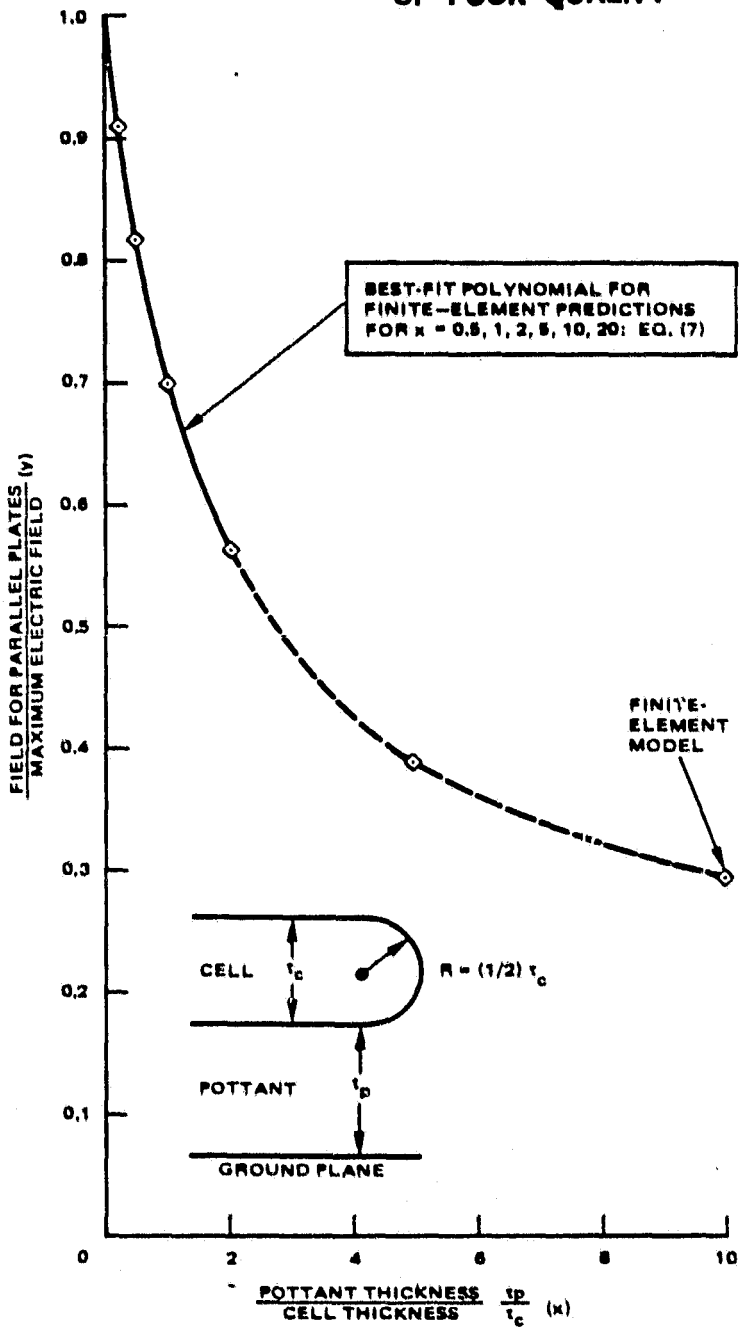

Figure 12. Disc-shaped cell — limit of electrical stress intensification factor as pottant becomes very thin.

to incur some numerical difficulties at $x = 0.25$, and it would take some labor to develop a model for this regime. We do not think that this is warranted, because accurate values of y for large values of t_c/t_p can be obtained by extrapolating the curve to (0,1). To demonstrate this, we fit the computed values for $0.5 \leq x \leq 20$ to a 5th degree polynomial. (We ignored the values for $x = 0.25$ and 50, for which the model is less accurate.) The best-fit formula was

$$y = 0.99279 - 0.409946\,x + 0.140055\,x^2 - 2.46179 \times 10^{-2}\,x^3 + 1.87591 \times 10^{-3}\,x^4 - 4.74338 \times 10^{-5}\,x^5 . \quad (7)$$

The index of determination was essentially unity, indicating that Eq. (7) is a very good fit. The curve resulting from this formula is smooth and monotonic for values of x as large as approximately 2. Therefore it can be used for predicting values of y not calculated by the finite-element model for $x \leq 2$. For values of x much larger than 2, the best-fit curve is oscillatory, characteristic of a high-degree polynomial. The important result for the present purpose is that the best-fit curve passes very close to (0,1) (actually it passes through (0,0.993)), even though we did not constrain the best-fit curve to pass through (0,1). This is strong evidence to support our hypothesis that the actual curve passes through (0,1).

The quantity of interest for the isolation design of a module is the maximum electric field E_m, which is given by Eq. (5). It can be written as

$$E_m = \frac{V_o/t_c}{yx} . \quad (8)$$

The maximum field can be evaluated from the finite-element results as follows. For a given applied voltage and cell thickness, E_m is a function only of the product yx, which is a function only of the module geometry. As an

example, consider the family of semicircular-edged solar cells shown in Figure 12. For this family, y is a function only of x. The product

$$yx = \frac{V_o/t_c}{E_m} \tag{9}$$

is plotted versus x in Figure 13. It is seen to be a monotonically increasing function of x for $x \leq 20$. Therefore the maximum electric field decreases with increasing pottant thickness, for pottant layers as much as 20 times thicker than the cell. It is recommended that this effort be continued to extend the finite-element model for values of $x \geq 20$, which are of interest for advanced thin-film devices. For comparison, the predictions of the series capacitance model also are shown in Figure 13. Because of the electrical stress intensification at the cell edges, the pottant has to be much thicker to reduce the maximum field to a given value than is predicted by the series capacitance model.

4.0 CONCLUSIONS

1) A finite-element method for evaluating the electrical-isolation characteristics of photovoltaic modules has been developed.

2) Its accuracy has been verified by comparison with an exact solution for a geometry similar to that of typical solar cells.

3) The utility of the finite-element method as a design tool has been demonstrated by the analysis of two sample geometries.

4) Accurate calculation of the maximum electric field required careful analysis. The finite-element models had to avoid large elements adjacent to small ones and had to avoid elements with large aspect ratios. The NASTRAN output had to be curve fit to calculate the maximum field accurately.

5) Larger, specially designed computer models would be required for the following three limits: cells having very sharp edges, cells much thinner than the dielectric pottant layer, and cells much thicker than the dielectric pottant layer.

5.0 RECOMMENDATION

The capability of the finite-element model should be extended to the geometries of advanced thin-film device modules.

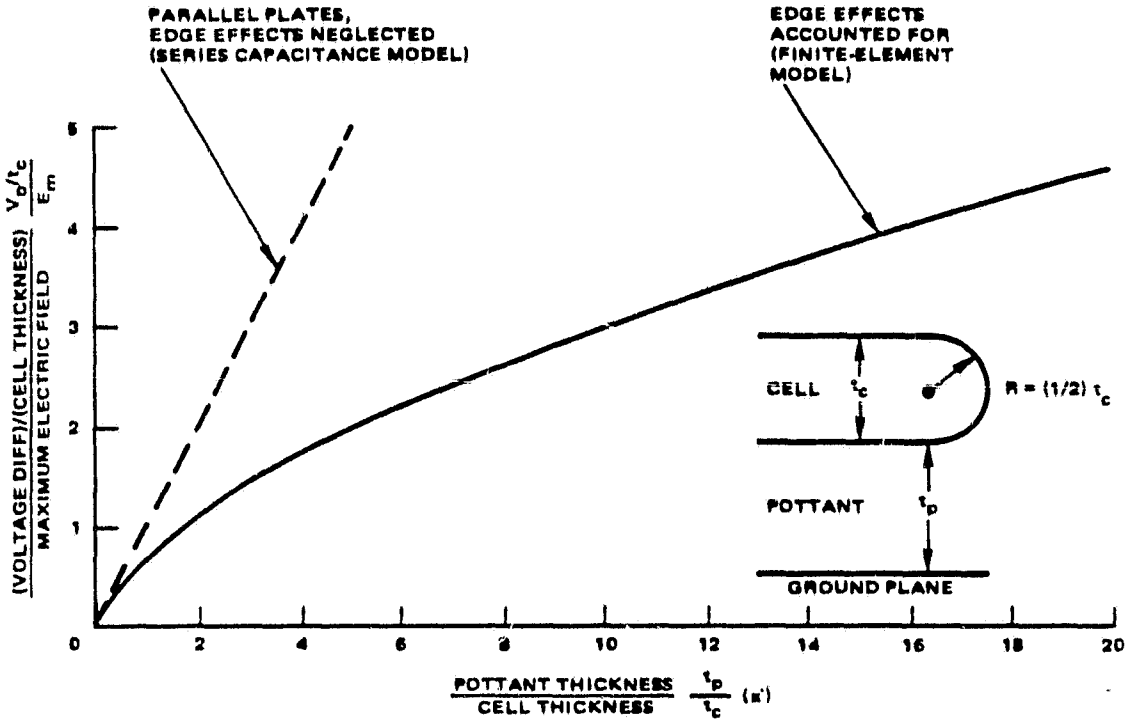

Figure 13. Disc-shaped cell — effect of pottant thickness on maximum electric field.

ACKNOWLEDGEMENTS

Technical discussions with C. D. Coulbert, E. F. Cuddihy, A. Garcia, W. W. McDonald, L. B. Duncan, and I. R. Jones were very helpful for the work described herein.

REFERENCES

1) LSA Engineering Area, "Low-Cost Array Project: Photovoltaic Module Design, Qualification and Testing Specification," JPL Report 5101-65, 24 March 1978.

2) LSA Engineering Area, "Low Cost Array Project: Photovoltaic Module Design, Qualification and Testing Specification," JPL Report 5101-83, 1 November 1978.

3) A. Garcia and C. P. Minning, "Design, Analysis, and Test Verification of Advanced Encapsulation Systems, Interim Report for Period Ending 1 October 1980," DOE/JPL-955567-81/4, November 1981.

4) "Analysis and Test Verification of Encapsulation Systems for Terrestrial Photovoltaic Modules", Hughes Aircraft Company Report No. FR 81-70-1091, October 1981.

4) G. R. Mon, "Defect Design of Insulation Systems for Photovoltaic Modules", Proc. 15th IEEE Photovoltaic Specialists Conf., pp. 964-971, May 1981.

6) M. V. K. Chari and P. O. Silvester (eds.), Finite Element in Electrical and Magnetic Field Problems, Wiley and Sons (U.K.), 1980.

7) D. K. Archipley-Smith and H. H. Fong, "Electrical and Thermostructural Analyses of Potted High-Voltage Electronic Devices", Proc. 1982 MSC/NASTRAN Users Conf.

8) J. R. Brauer, "Finite Element Analysis of Electric and Magnetic Fields", First Chautauqua on Finite Element Modeling (ed. J. H. Conaway), sponsored by Schaefer Analysis, Inc., 1980.

9) H.-P. Lee, "NASTRAN Thermal Analyzer — Theory and Application Including a Guide to Modeling Engineering Problems, Vol. 1", N77-23411, April 1977.

APPENDIX A

DEVELOPMENT OF NUMERICAL METHOD FOR CALCULATING MAXIMUM ELECTRIC FIELD

This appendix elaborates on the description in Section 2.2 of the method for calculating the maximum electric field.

Figure A-1 shows the output of a typical NASTRAN run. It consists of the potential at each grid point in the finite-element model. For this geometry, the maximum potential gradient occurs on the surface normal denoted by grid points 1, 2, 3, and 4. The maximum field, which occurs at the cell surface (grid point 1), is given by

$$E_m = \left.\frac{dV(D)}{dD}\right|_{D=0} \tag{A1}$$

The actual function V(D) (the solid curve in the figure) is seen to have a non-zero second derivative. NASTRAN, however, calculates the field simply by fitting a straight line through adjacent grid points:

$$E_m = \frac{V_2 - V_1}{D_2 - D_1} \text{ (NASTRAN)} \tag{A2}$$

Comparison of the two dashed lines in the figure showed that the straight-line approximation underestimated the surface gradient by 6%. The difference between the two values of the surface gradient was 10-20% for many of the other geometries analyzed in this project. The error in the surface gradient resulting from the straight-line approximation was difficult to detect by visual inspection of the graph, but it showed up when surface gradients were calculated. To improve the accuracy, we tried 1) using a finer computational mesh and 2) modifying the shape of the mesh. Neither modification yielded adequate accuracy, because Eq. (A2) inherently underestimates the surface gradient.

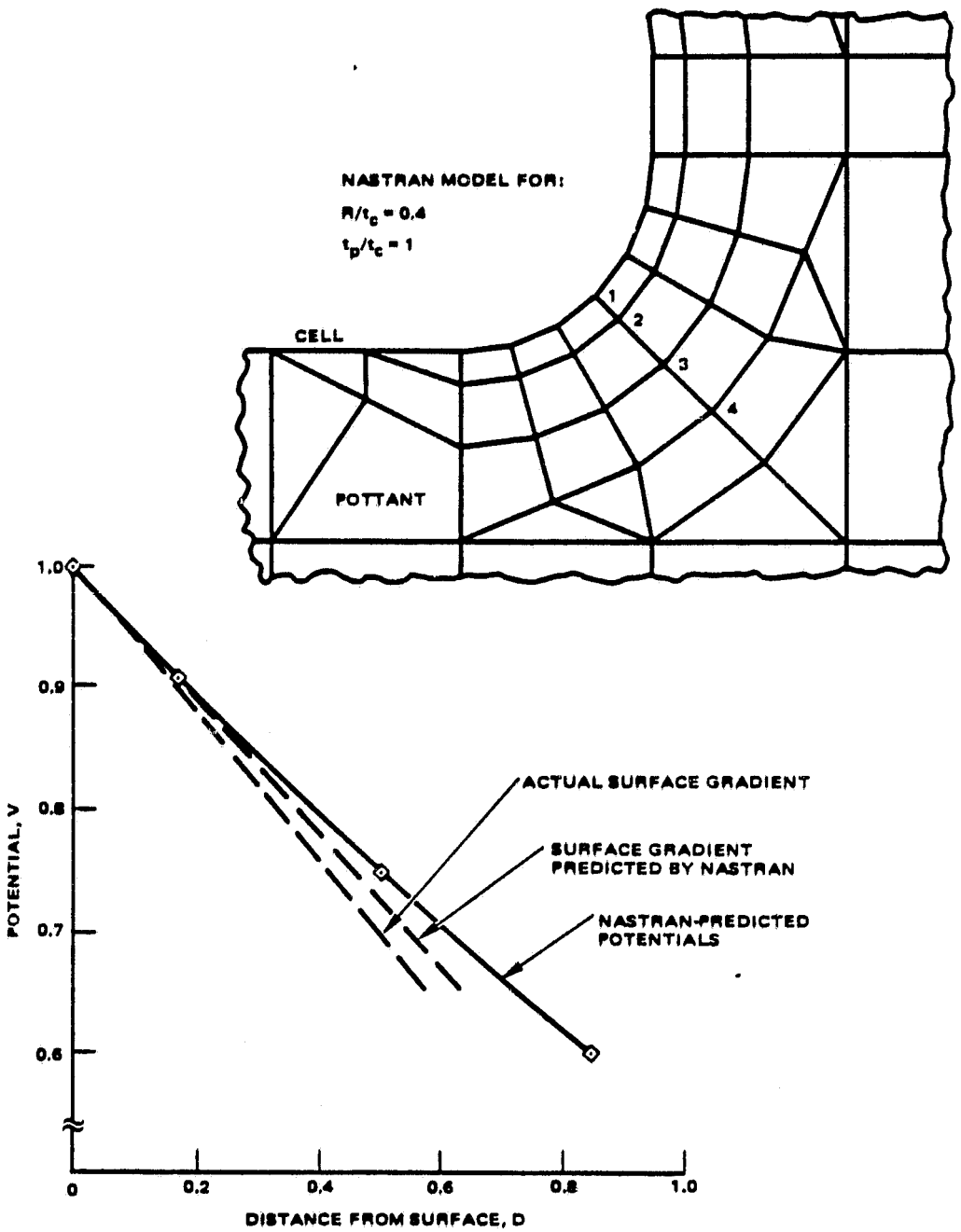

Figure A-1. Underestimation of maximum field by NASTRAN illustrating need to post-process output data.

Accurate values finally were obtained by post-processing the NASTRAN output. The first step was to determine the direction of the maximum surface gradient by inspection of the NASTRAN output. Then the 4th-degree polynomial that was the best fit to the function V(D) along this direction was determined by the method of least squares. The curve fit used the potentials at four or five grid points, depending on the geometry. Then the surface derivative was evaluated from the best-fit polynomial and equated to the maximum field, per Eq. (A1). With this post-processing, a moderate-size (around 500 elements) NASTRAN model provided sufficient accuracy, except for extreme geometries discussed in the next paragraph. As mentioned in Section 2.3, the maximum field predicted by this method agreed very closely with that calculated from the exact solution for a geometry for which an exact solution of Laplace's equation exists.

Even with this method, however, care is required in developing the finite-element model to obtain accurate results. Analysts should pay special attention to 1) the fineness of the computational mesh and 2) the shapes of the finite elements. A fine mesh is required in regions having large gradients, such as near edges and corners. But the analyst must take care to gradually make the mesh coarser with increasing distance from the edge or corner. We found that a model having a large element adjacent to a small one gave inaccurate results. NASTRAN also incurs numerical difficulties with models having elements with aspect ratios greater than about 1,500:1. Therefore elements with large aspect ratios should be avoided. For these reasons, models of 1) edges or corners with very small radii of curvature, 2) very thin cells, or 3) very thin dielectric pottant layers must be very large and thus expensive.

APPENDIX B

EXACT SOLUTION FOR BLUNTED KNIFE-EDGED SLAB

The geometry for which the exact solution, described in Section 2.3, exists is shown in Figure B-1. The geometry is planar and is specified by Cartesian coordinates u and v. The ground planes are located at v = 0 and v = π. The other electrode, at which V = 1, is located at v = π/2 for u ≥ 0.

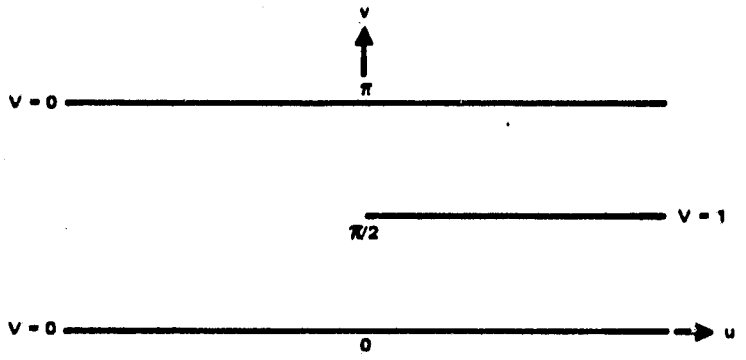

Figure B-1. Configuration for exact solution.

The potential function in the region between the ground planes can be determined by conformal mapping, using the Schwarz-Christoffel transformation. The solution is (Reference B1)

$$T = (e^{-4u} - s^2)^{1/2}/s, \tag{B1}$$

where

$$T = \tan \pi V, \tag{B2}$$

$$s = -1 + (1 + 2e^{-2u} C + e^{-4u})^{1/2}, \tag{B3}$$

and

$$C = \cos 2v. \tag{B4}$$

The quantity s is positive for $V < 1/2$, zero for $V = 1/2$, and negative for $V > 1/2$.

The equipotential surfaces have the shapes shown in Figure B-2. They are blunted knife-edged slabs. The edge is located at the point $(u_o, \pi/2)$, where

$$e^{-2u_o} = \frac{2(1 + T^2)^{1/2}}{T^2} \left[(1 + T^2)^{1/2} + \text{sign}(s)\right]. \tag{B5}$$

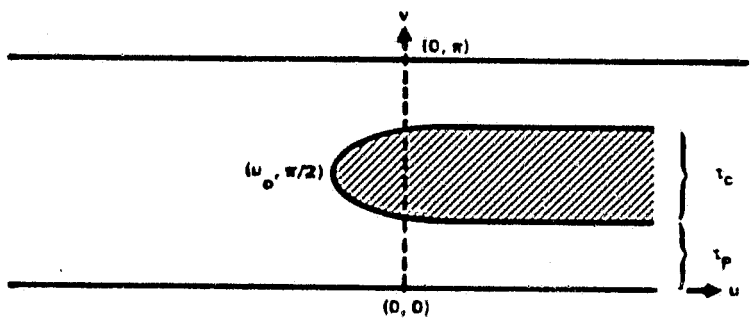

Figure B-2. Equipotentials.

Each surface approaches a pair of parallel planes as $u \to \infty$, that is,

$$\lim_{u \to \infty} T = \pm \tan 2v. \tag{B6}$$

Therefore

$$\lim_{u \to \infty} v = \begin{cases} \pi - \frac{\pi}{2} V, & v > \frac{\pi}{2} \\ \\ \frac{\pi}{2} V, & v < \frac{\pi}{2} \end{cases} . \tag{B7}$$

Thus an equipotential surface can be thought of as a solar cell having a thickness

$$t_c = \left(\pi - \frac{\pi}{2} V\right) - \frac{\pi}{2} V = \pi(1 - V) \tag{B8}$$

encapsulated in a dielectric pottant having a thickness

$$t_p = \frac{\pi}{2} V. \tag{B9}$$

Therefore

$$\frac{t_c}{t_p} = 2 \frac{1 - V}{V} . \tag{B10}$$

The value $V = 1/2$ corresponds to $t_c/t_p = 2$. The electric field approaches the asymptotic value

$$E_\infty = \lim_{u \to \infty} E\ (u,v) = \frac{V}{t_p} = \frac{2}{\pi} . \tag{B11}$$

The magnitude of the electric field vector is given by

$$E = [(\partial V/\partial u)^2 + (\partial V/\partial v)^2]^{1/2}. \tag{B12}$$

By evaluating these derivatives, the electric field can be written simply as

$$E = \frac{2/\pi}{(s + 1)^{1/2}}. \tag{B13}$$

The maximum field E_m is determined as follows. For $V \leq 1/2$, $s \geq 0$. Therefore the maximum field occurs where $s = 0$. From Eq. (B3), $s = 0$ at $u = \infty$. Therefore $E_m = E_\infty$ and is given by Eq. (B11). In other words, the electric field does not exceed the parallel-plate value in the region where $V \leq 1/2$. For $V > 1/2$, $s \leq 0$. Therefore the maximum field occurs where s has its minimum value. From Eqs. (B1) - (B3), we have

$$s = 2[1 + (1 + T^2)^{1/2}C]/T^2. \tag{B14}$$

The quantity $T = \tan \pi V$ is constant on an equipotential surface. The quantity $C = \cos 2v$ can vary between the values -1 and 1. The minimum value of s occurs where $C = -1$ (that is, at $v = \pi/2$) and is given by

$$s_m = 2[1 - (1 + T^2)^{1/2}]/T^2. \tag{B15}$$

Therefore the maximum field is given by

$$E_m = \left\{ \begin{array}{ll} 2/\pi & , V \leq 1/2 \\ \dfrac{2/\pi}{(s_m + 1)^{1/2}} & , V > 1/2 \end{array} \right\}. \tag{B16}$$

The electrical stress intensification factor y, defined by

$$y = E_\infty / E_m \ , \tag{B17}$$

is given from Eqs. (B11) and (B16) by

$$y = \left\{ \begin{array}{ll} 1 & , \ V \leq 1/2 \\ (s_m + 1)^{1/2} & , \ V > 1/2 \end{array} \right\} . \tag{B18}$$

It is plotted versus t_c/t_p in Figure B-3.

REFERENCE

B1) R. V. Churchill, Complex Variables and Applications, 2nd ed., pp. 237-240, McGraw-Hill Book Co., New York, 1960.

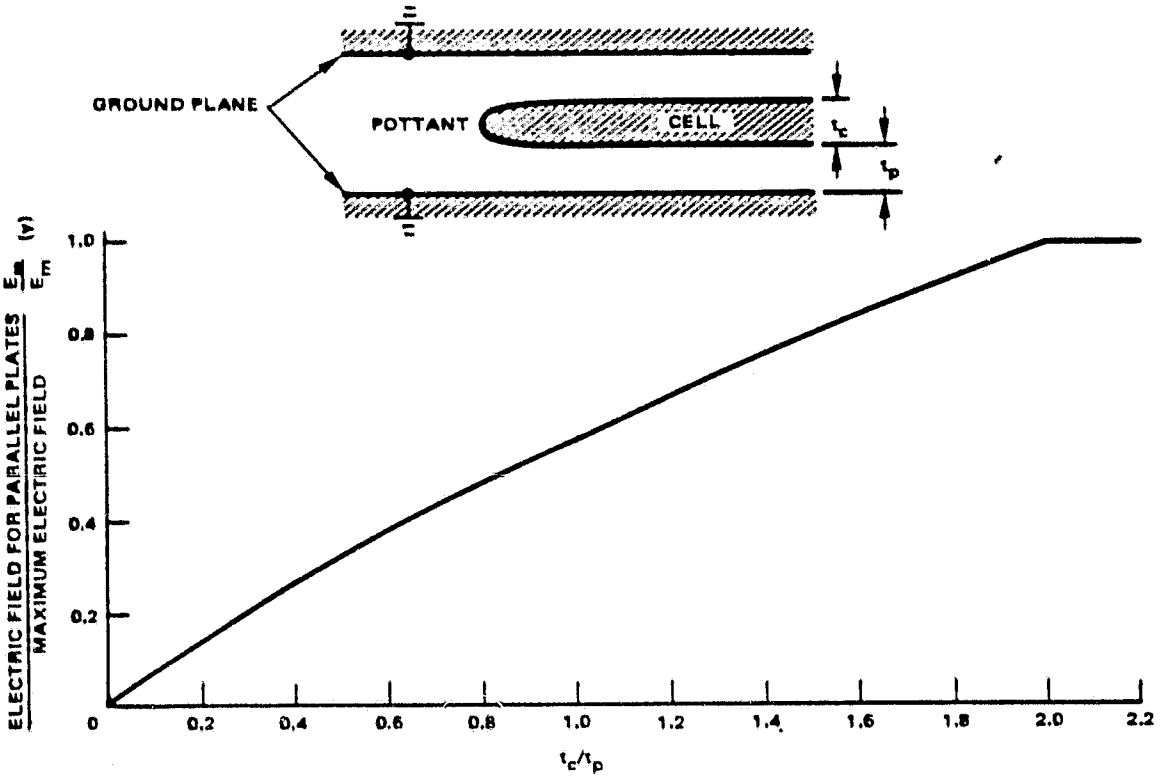

Figure B-3. Electrical stress intensification factor for blunted knife-edged slab (exact solution).